A scanning Hall probe imaging study of the field induced martensite–austenite phase transition in $Ni_{50}Mn_{34}In_{16}$ alloy

2010 J. Phys.: Condens. Matter 22 016008

(http://iopscience.iop.org/0953-8984/22/1/016008)

J. Phys.: Condens. Matter **22** (2010) 016008 (8pp) doi:10.1088/0953-8984/22/1/016008

A scanning Hall probe imaging study of the field induced martensite–austenite phase transition in $Ni_{50}Mn_{34}In_{16}$ alloy

V K Sharma[1], J D Moore[2], M K Chattopadhyay[1], Kelly Morrison[2], L F Cohen[2] and S B Roy[1]

[1] Magnetic and Superconducting Materials Section, Raja Ramanna Centre for Advanced Technology, Indore 452013, India
[2] The Blackett Laboratory, Imperial College London, London SW7 2AZ, UK

Received 3 July 2009, in final form 30 September 2009
Published 3 December 2009
Online at stacks.iop.org/JPhysCM/22/016008

Abstract

The martensite to austenite phase transition in the off-stoichiometric Heusler alloy $Ni_{50}Mn_{34}In_{16}$ can be induced both by temperature change and by application of a magnetic field. We have used scanning Hall probe imaging to study the magnetic field induced martensite–austenite phase transition. The study provides clear visual evidence of the coexistence of the martensite and austenite phases across this field induced transition in both increasing and decreasing magnetic fields. Clear evidence of thermomagnetic history effects associated with the martensite–austenite phase transition is also obtained. Quantitative analysis of the magnetic field dependence of the volume fraction of the austenite phase in $Ni_{50}Mn_{34}In_{16}$ shows evidence of a nucleation and growth mechanism across the field induced martensite–austenite phase transition. The local M–H loops constructed from the Hall images indicate the presence of a landscape of the critical magnetic field (for the field induced transition) distributed over the sample volume and thus confirm the disorder influenced nature of this first-order magnetic phase transition.

(Some figures in this article are in colour only in the electronic version)

1. Introduction

Recently, the off-stoichiometric Heusler alloys $Ni_{50}Mn_{50-x}In_x$ have drawn considerable attention due to their potential as ferromagnetic shape memory alloys [1–4]. These alloys undergo a martensitic transition from the high temperature austenite (AST) phase to the low temperature martensite (MST) phase with the lowering of temperature [1]. The reverse transition from the MST to the AST phase can be induced by changing temperature (T) as well as by applying a magnetic field (H) [1–10]. The $x = 16$ composition of this alloy system, i.e., the $Ni_{50}Mn_{34}In_{16}$ alloy, exhibits a paramagnetic to ferromagnetic transition near 305 K, followed by a martensitic transition near 220 K with the lowering of temperature [1, 3–10]. The $Ni_{50}Mn_{34}In_{16}$ alloy exhibits various interesting and technologically important physical properties, e.g. large magnetoresistance [4, 5], a large magnetocaloric effect [6–8] and magnetic superelasticity [7]. These multifunctional properties are attributes of the magnetic field induced MST to AST phase transition in this alloy.

Magnetization [10] and resistivity [4] measurements performed earlier have revealed clear thermomagnetic hysteresis across the temperature and field induced MST–AST transition in $Ni_{50}Mn_{34}In_{16}$ alloy. Such thermomagnetic hysteresis is a generic feature of a disorder influenced first-order phase transition and has been observed in various classes of magnetic systems undergoing a first-order magnetostructural phase transition [11]. Scanning Hall probe imaging experiments have been very useful in the investigation of such magnetic systems, revealing clear phase coexistence and metastability across the first-order phase transition [12, 13]. In this work we probe the field induced MST to AST transition in $Ni_{50}Mn_{34}In_{16}$ alloy using scanning Hall probe imaging experiments. To the best of our knowledge, this is the first report of scanning Hall probe imaging of a field induced MST–AST phase transition in such multifunctional Heusler alloys. The scanning Hall probe images clearly show the coexistence of MST and AST phases across this field induced transition and provide visual evidence of thermomagnetic hysteresis, implying that the transition is indeed first order in nature. The magnetic field

dependence of the volume fraction of the AST phase fits with an equation representing the Kolmogorov–Johnson–Mehl–Avrami (KJMA) relation [14] (proposed for crystallization of solids), which suggests an underlying nucleation and growth mechanism of the transition. The local M–H loops constructed from the Hall images indicate the presence of a landscape of critical fields (for the MST–AST transition) distributed over the sample volume and thus confirm the disorder influenced nature of the transition. In addition, the present results explain why the functional properties (magnetoresistance and magnetocaloric effect) of $Ni_{50}Mn_{34}In_{16}$ depend on the thermomagnetic history of the sample.

2. Experimental details

The nominal alloy composition $Ni_{50}Mn_{34}In_{16}$ was prepared by arc melting the appropriate amount of constituent pure elements under an inert argon gas atmosphere. The sample ingot was flipped and re-melted several times to ensure homogeneity. The sample was characterized via x-ray diffraction (XRD) study. XRD results indicated an $L2_1$ ordering. The actual composition of the sample was determined as $Ni_{49.2}Mn_{34.7}In_{16.1}$ with energy dispersive x-ray analysis (EDX). Portions of the same sample have been used in previous experiments [4, 6, 9, 10]. Measurements of the magnetization (M) as a function of temperature and magnetic field were performed using a superconducting quantum interference device (SQUID) magnetometer (MPMS-5, Quantum Design) and a vibrating sample magnetometer (VSM, Quantum Design). The temperature dependence of the magnetization was studied using the following protocols.

(i) The field cooled cooling (FCC) protocol, where the magnetic field is applied in a temperature regime well above the Curie temperature of the sample and the measurements are performed in the presence of the applied magnetic field while cooling the sample down to the lowest temperature of measurement.

(ii) The field cooled warming (FCW) protocol, where the sample is first cooled down to the lowest temperature of measurement in the FCC mode, and then the measurements are made in the presence of the same applied magnetic field while warming up the sample.

The scanning Hall probe imaging was performed using a custom built scanning Hall probe set-up [15] with a 5 μm InSb Hall sensor. The sample used in this study has a surface area approximately 2 mm × 2 mm with a thickness of 1 mm approximately, and each Hall image consists of 256 pixels × 256 pixels. The Hall voltage profiles, recorded while scanning the sample surface, were converted to a multi-tone image where bands of tone are assigned to different Hall voltage ranges. The integrated moment in a particular magnetic field was calculated by summing the Hall voltage from all the pixels in the Hall image in that field.

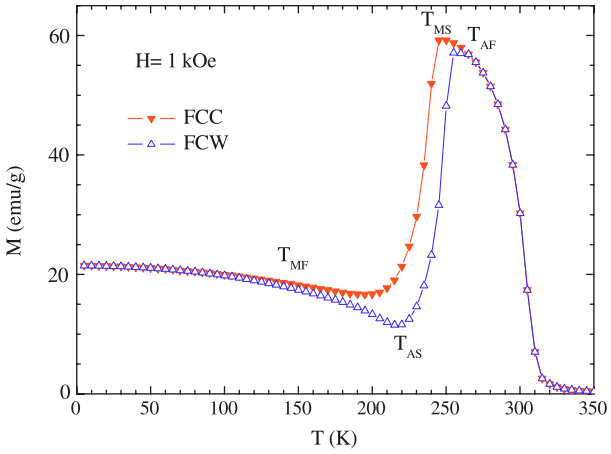

Figure 1. Temperature (T) dependence of the magnetization (M) for $Ni_{50}Mn_{34}In_{16}$ alloy in a magnetic field (H) of 1 kOe.

3. Results and discussion

Before presenting the results of the scanning Hall probe imaging measurements, it will be instructive to prepare an H–T phase diagram based on some representative isothermal and constant field magnetization measurements. This helps in identifying the appropriate H–T region for imaging with the scanning Hall probe, and also makes the present work self-contained. Figure 1 presents magnetization versus temperature curves for $Ni_{50}Mn_{34}In_{16}$ alloy measured in a 1 kOe magnetic field. The rise in magnetization with the lowering of temperature near $T \approx 305$ K is related to the paramagnetic to ferromagnetic transition in this alloy, and the drop in magnetization near 240 K with further lowering of the temperature corresponds to the AST to MST transition. The thermal hysteresis associated with this AST–MST transition is an attribute of the first-order nature of the transition [16]. It is worth noting here that the excess Mn atoms present in this off-stoichiometric Heusler alloy $Ni_{50}Mn_{34}In_{16}$, compared to the stoichiometric alloy $Ni_{50}Mn_{25}In_{25}$, occupy a number of 4(b) sites in the $L2_1$ structure [17, 18]. In the literature there is a suggestion of an incipient antiferromagnetic coupling in these Mn atoms which probably becomes stronger in the MST phase [17, 18]. This probably causes the large drop in magnetization from the AST to the MST phase. However, both the AST and the MST phases of the alloy have an overall ferromagnetic order, but with different microscopic characters [19].

It is observed in figure 1 that, unlike the sharp transition at one temperature expected for an ideal first-order transition [20], the AST to MST and MST to AST phase transitions are spread over a finite temperature width, indicating a disorder broadened nature of the transition [21]. Quenched random disorder (structural, compositional, microstrain related, etc) in the sample produces a landscape of transition temperatures spreading over the bulk of the sample [12, 22–24]. This landscape picture along with the characteristic hysteresis of the first-order phase transition [16] leads to the occurrence of characteristic onset and completion temperatures for both the AST to MST and

the MST to AST phase transitions in $Ni_{50}Mn_{34}In_{16}$ alloy. The characteristic temperatures of the AST–MST phase transition in the present case are defined as follows. The temperature at which the AST to MST phase transition starts with decreasing temperature is denoted as T_{MS}. On the other hand, T_{MF} characterizes the temperature at which this transition is completed (see figure 1). Similarly, T_{AS} and T_{AF} define the start and finish temperatures for the MST to AST phase transition with increasing temperature. The whole sample is in the AST (MST) phase at temperatures higher (lower) than T_{MS} (T_{MF}) in the temperature decreasing cycle. Similarly, the whole sample is in the MST (AST) phase at temperatures lower (higher) than T_{AS} (T_{AF}) in the temperature increasing cycle. At the temperature T_{MF} (T_{AF}) the FCC (FCW) curve merges with the FCW (FCC) curve in the temperature region below (above) the temperature regime of the MST–AST transition (see figure 1). We have taken the temperature value where the FCC (FCW) curve visually merges (see figure 1) with the FCW (FCC) curve as T_{MF} (T_{AF}). This corresponds to the criterion that the difference between the magnetizations along the FCC and FCW curves decreases to 1% of the maximum magnetization in the graph. In this picture, in the temperature range T_{MS}–T_{MF} (T_{AS}–T_{AF}) in the temperature decreasing (increasing) cycle both the MST and the AST phases should coexist. The temperatures T_{MF} and T_{AF} actually correspond to the temperatures T^* and T^{**} respectively, representing the limits of supercooling and superheating of the temperature driven first-order phase transition [16]. In other words, T_{MF} is the limit of supercooling of the austenite phase and T_{AF} is the limit of superheating of the martensite phase. In the rest of the paper we shall use T^* and T^{**} instead of T_{MF} and T_{AF} to represent the MST and AST finish temperatures. It is worth noting that in the present case $T_{MS} > T_{AS}$. Only the presence of a landscape of transition temperature over the sample volume can lead to such a relationship between the temperatures T_{MS} and T_{AS} [23].

In isothermal magnetic field variation a first-order field induced transition from the MST to the AST phase has been observed in $Ni_{50}Mn_{34}In_{16}$ alloy [6, 19]. The characteristic features of this field induced transition are quite similar to those observed in various other systems undergoing field induced metamagnetic transition, e.g., $CeFe_2$ alloys [12, 23, 25], Gd_5Ge_4 [26], doped Mn_2Sb [27] and MnAs [28]. Like the temperature induced transition, the magnetic field induced transition in $Ni_{50}Mn_{34}In_{16}$ alloy also has a finite field width [19]. From arguments similar to that used in the case of temperature induced transition, this may be related to the presence of disorder in the sample which leads to a landscape of onset fields of the phase transition. Analogously the characteristic magnetic fields are defined in the following way: H_A characterizes the magnetic field at which the transition from the MST to AST phase starts in increasing magnetic field. The field at which this MST to AST phase transition is completed is denoted by H^{**}. In the decreasing magnetic field cycle, the magnetic field value at which the AST to MST phase transition starts is denoted by H_M. The magnetic field at which this AST to MST phase transition is completed is denoted as H^*. The whole sample is in the MST phase at a given temperature in magnetic fields below H_A. The MST

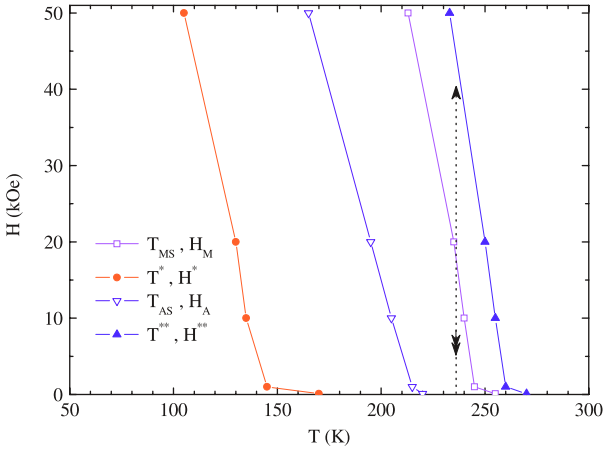

Figure 2. The H–T phase diagram of $Ni_{50}Mn_{34}In_{16}$ alloy. The dotted line in the H–T phase diagram depicts the path on which the scanning Hall probe imaging experiments were performed in the increasing and decreasing magnetic field cycles at 236 K. The single arrowhead shows the increasing field path and the double arrowhead shows the decreasing field path.

and AST phases should coexist in the magnetic field range H_A–H^{**} in the increasing magnetic field cycle. The whole sample is in the AST phase in magnetic fields higher than H^{**}. Similarly in the decreasing magnetic field cycle the whole sample is in the AST phase down to the magnetic field H_M. In the magnetic field range H_M–H^* the AST and MST phases should coexist, and in magnetic fields lower than H^* the whole sample is in the MST phase, in the decreasing magnetic field cycle. Thus, H^* and H^{**} respectively represent the limits of supercooling and superheating for the field induced first-order MST–AST phase transition. In magnetic field higher (lower) than H^{**} (H^*), the isothermal M versus H curves along increasing and decreasing magnetic field cycles merge with each other. These characteristic temperatures and magnetic fields can also be obtained from temperature variation of the resistivity in constant fields [4] or isothermal field variation of the resistivity [29]. The experimental H–T phase diagram of the present $Ni_{50}Mn_{34}In_{16}$ alloy obtained from the results of magnetization [19] and resistivity measurements [4] is presented in figure 2.

We now study the field induced MST–AST phase transition in the $Ni_{50}Mn_{34}In_{16}$ alloy using the scanning Hall probe imaging technique. We have chosen 236 K as the most appropriate temperature for capturing images of the transition as this temperature is within the MST–AST phase coexistence regime (see figure 2). Also, the maximum magnetic field that can be applied in our scanning Hall probe imaging experimental set-up is 40 kOe. At 236 K, the field induced transition is nearly completed in a 40 kOe magnetic field [19]. Two different protocols were adopted to reach the temperature 236 K.

(i) In the protocol P1, the sample was cooled from 300 K in zero magnetic field down to 236 K without undershooting the target temperature. The scanning Hall probe imaging experiments were performed at constant temperature first

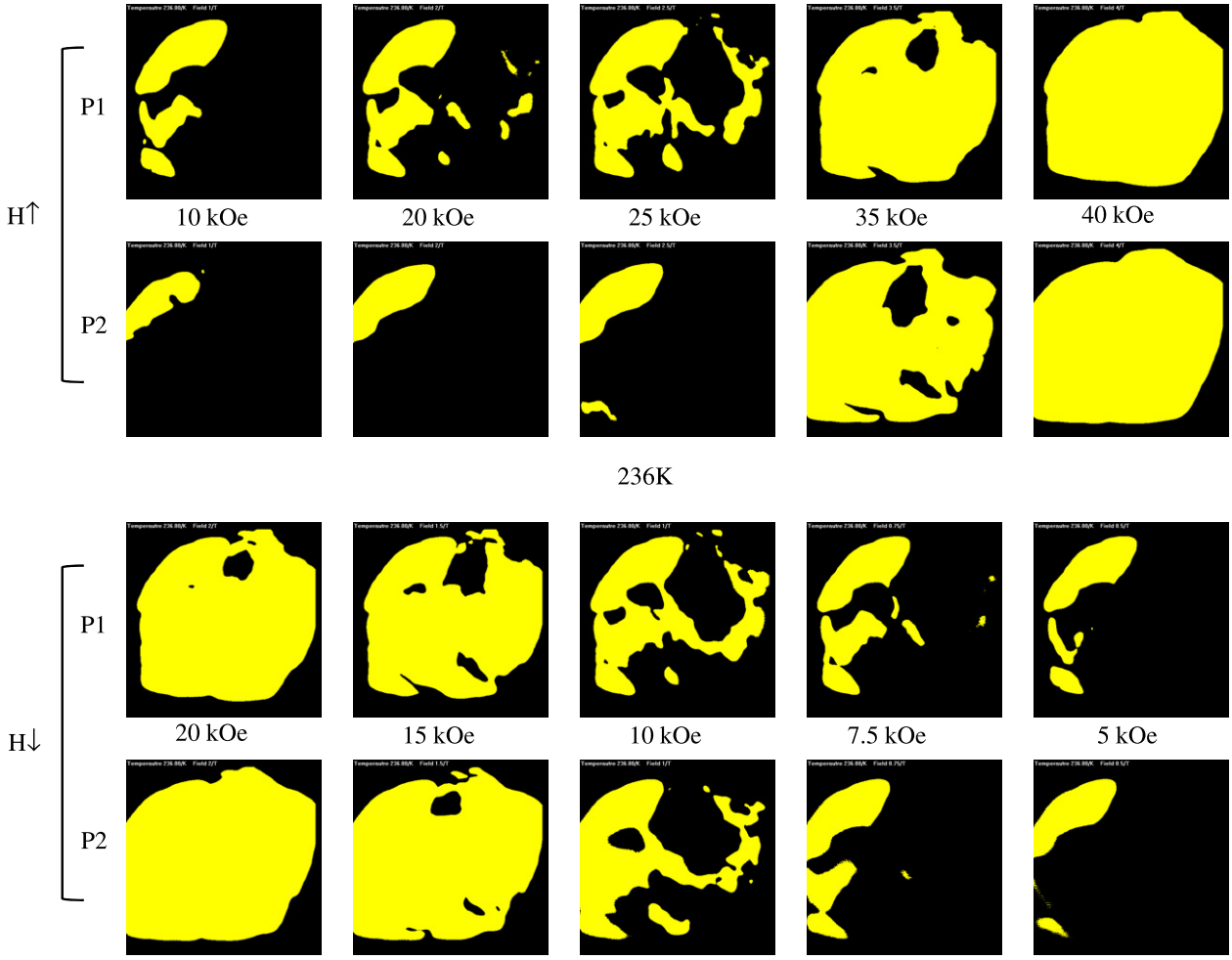

Figure 3. Scanning Hall probe images of the $Ni_{50}Mn_{34}In_{16}$ alloy in different magnetic fields at 236 K in two different protocols, P1 and P2. The Hall images were taken in increasing ($H\uparrow$) and decreasing ($H\downarrow$) magnetic field cycles. In the Hall images, the yellow regions represent the austenite phase and the black regions represent the martensite phase. The region beyond the sample edges is also black.

in the increasing magnetic field cycle (up to 40 kOe) and then in the decreasing magnetic field cycle (down to zero).

(ii) In the protocol P2, the sample was cooled in zero magnetic field from 300 to 30 K. Then the sample was warmed up to 236 K without overshooting the target temperature, and subsequently the scanning Hall probe imaging was performed at constant temperature in the increasing and decreasing magnetic field cycles.

We have seen that the magnetization of the MST phase is lower than that of the AST phase. To differentiate between the MST and AST phases in the Hall voltage profile we have chosen a voltage threshold such that the voltages below this threshold represent the MST phase, and the voltages higher than this threshold represent the AST phase. Since the magnetic field induced MST to AST transition is nearly complete in 40 kOe magnetic field at 236 K, we have taken the whole sample to be in the AST phase in 40 kOe field at this temperature. We have taken the Hall voltage threshold at 50% of the maximum in the Hall voltage profile in 40 kOe magnetic field. The same voltage threshold has been used in both the protocols P1 and P2. The colour figures thus obtained in both the protocols in the increasing ($H\uparrow$) and decreasing magnetic field ($H\downarrow$) cycles are shown in figure 3. Here, the yellow regions represent the AST phase, and the black regions represent the MST phase. The field of view for imaging was larger than the sample size. Once the background (due to the applied field) was removed, this also produced a black region around the periphery of the sample which simply defines the edge of the sample.

As the magnetic field is increased from zero to 10 kOe at 236 K, some portions of the images show yellow colour, indicating that the MST to AST phase transition has started in these regions of the sample. From figure 3 it is clearly seen that the amount of the AST phase in $H = 10$ kOe is larger in protocol P1. With increasing magnetic field, newer yellow patches come up and the existing yellow patches grow in area, indicating the nucleation and growth of the AST phase. Finally the entire sample is yellow in 40 kOe magnetic field for both the protocols P1 and P2. However, the nucleation and growth kinetics of the MST to AST phase transformation is slower in the protocol P2 for fields up to 25 kOe. Above this field, the MST to AST phase transformation is much faster in the protocol P2 as compared to the protocol P1. In the decreasing field cycle, the MST phase appears as black spots and the nucleation and growth of the MST phase are

clearly seen in the lower panel of figure 3. The nucleation and growth kinetics of the AST to MST phase transformation in the protocols P1 and P2 appear to be quite similar as the field is decreased from 40 kOe to zero. The transformation becomes quite slow in the low fields and some AST phase remains untransformed in fields down to 5 kOe in both the protocols. Thus figure 3 actually shows snapshots of the coexistence of MST and AST phases on the length scale of tens of micrometres, extended over a very wide regime of magnetic field. Comparison of the top and bottom panels of figure 3 also confirms the magnetic field hysteresis associated with this field induced transition (for example compare the Hall images taken in 20 kOe magnetic field, in the increasing and decreasing field cycles). It is also observed in figure 3 that the region of sample where the MST to AST phase transition starts first (last) in the increasing magnetic field cycle is also the region where the AST to MST transition starts last (first) in the decreasing magnetic field cycle. This shows that the hysteresis associated with the field induced MST–AST phase transition is influenced by microscopic characteristics (disorder, strain, etc) specific to particular microscopic regions of the sample.

To investigate further the field induced MST–AST phase transition, we estimate the volume fractions of the AST and MST phases as a function of magnetic field in both the protocols. In figure 3, the area of the yellow region in the images is a measure of the volume fraction of the AST phase (VF_{AST}). To calculate VF_{AST}, we normalize the area of the yellow region in an image with the area of the yellow region in the scanning Hall probe image obtained in 40 kOe magnetic field. The volume fraction of the MST phase (VF_{MST}) is related to VF_{AST} through the relation $VF_{AST}(\%) + VF_{MST}(\%) = 100$. The volume fraction thus calculated is not an exact quantitative estimate since the MST and AST microregions beneath the surface of the sample also contribute to the Hall voltage profile to varying degrees depending on their depth. Hence the VF_{AST} estimated from Hall images is only representative of the actual phase distribution in the bulk sample. The contribution from the MST/AST regions to the Hall voltage profile also depends on their length scale relative to the resolution of the Hall probe. If the length scale of MST–AST phase coexistence is smaller than the resolution of the scanning Hall probe (nearly 10 μm in the present case), the probe will sense effective magnetization averaged over a pixel. This also contributes to the uncertainty in the estimated VF_{AST}. Moreover, at low magnetic fields the local magnetization may not be fully aligned with the field due to anisotropy and/or domain wall pinning, and our scanning Hall probe senses the component of local magnetic induction perpendicular to the sample surface. Nevertheless we are able to make qualitative measurements of the behaviour across this field induced transition.

The magnetic field dependence of the volume fractions of AST and MST is presented in figure 4. As indicated by Hall images taken in 10 kOe magnetic field in the increasing magnetic field cycle, the amount of AST phase is larger in protocol P1. The difference in kinetics of the martensite to austenite phase transition between the protocols P1 and P2 with increasing magnetic field is clearly seen in figure 4. With decreasing magnetic field there is very little change in VF_{AST}

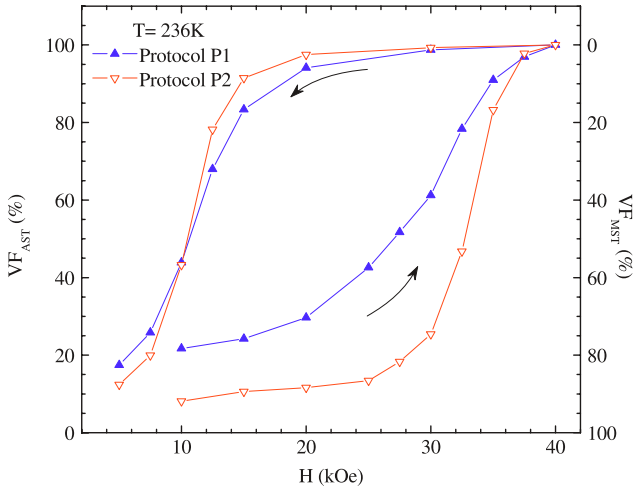

Figure 4. Isothermal magnetic field (H) dependence of the volume fraction of the austenite (VF_{AST}) and martensite (VF_{MST}) phases in $Ni_{50}Mn_{34}In_{16}$ alloy at 236 K in two different protocols. See the text for details.

until 20 kOe is reached, and below this magnetic field the rate of change of VF_{AST} is enhanced appreciably. The field dependences of VF_{AST} with decreasing magnetic field for the two protocols P1 and P2 are qualitatively similar, which is in contrast with the increasing field cycle case discussed above.

In our earlier work we found that the $M(H)$ behaviour of $Ni_{50}Mn_{34}In_{16}$ across the AST–MST phase transition and the magnetocaloric effect exhibited by this alloy sample across this phase transition are strongly dependent on the experimental protocol [10, 30]. The giant magnetoresistance exhibited by this alloy sample [4] is also found to exhibit a similar dependence on the experimental protocol [4, 31]. These observations suggest that the kinetics of the magnetic field induced MST to AST transition in the $Ni_{50}Mn_{34}In_{16}$ alloy is affected by the thermomagnetic history of the sample. The protocols P1 and P2 were adopted to investigate visually the effects of such thermomagnetic history on the field induced transition in this alloy. In the protocol P2, 236 K is reached after crossing the T_{AS} or H_A line. As this line is crossed, the MST to AST phase transformation is initiated. At 236 K, the AST phase is the equilibrium configuration at $H = 0$, and the MST phase is metastable (superheated) [16]. As the field is raised above 30 kOe under the protocol P2, the system goes very close to the limit of superheating [16] T^{**} or H^{**}. The rate of the MST to AST transformation is very high in this field regime and this is in harmony with our earlier finding that the rate of a first-order magnetic phase transformation increases rapidly when the system goes close to the spinodal limit [23, 32]. This phenomenon has earlier been observed across the first-order antiferromagnetic–ferromagnetic phase transition in 4% Ru doped $CeFe_2$ alloy [23] and across a field induced first-order phase transition in vortex matter [32]. In the protocol P1, on the other hand, 236 K is reached after crossing the T_{MS} or H_M line. At $H = 0$ and $T = 236$ K in the protocol P1, part of the sample is in the equilibrium MST phase and the remaining part is in the supercooled (metastable) [16] AST phase. As the field is increased, however, the situation

is changed altogether. The system now moves towards the limit of superheating [16] of the MST phase. In this route the AST phase is the equilibrium state, and the MST phase is metastable. The field increasing path in protocol P1 causes a kind of reversal of the kinetics of the phase transition, and thus probably introduces a large disturbance in the system. This kinetics is different from that of protocol P2, and accordingly, the behaviour of the system in protocol P1 is different from that of P2 in the field increasing cycle. In both the protocols P1 and P2, the system is very close to the limit of superheating (T^{**} or H^{**}) at $H = 40$ kOe. When the field is decreased from 40 kOe, there is no path difference (in the H–T phase space) between the two protocols and accordingly the kinetics of the phase transition in the two protocols are similar (figures 3 and 4). The AST to MST phase transition is initiated below 20 kOe when the system crosses the T_{MS} or H_M line in both the protocols. The present scanning Hall probe microscopy images show that the dependence of the functional properties of the alloy on the protocol used for changing the field and temperature is because of the relative volume fractions of the MST and AST phases present in the alloy. It is clear from figures 3 and 4 that these volume fractions are strongly dependent on the path traversed by the system in the H–T phase space.

It is observed in figure 4 that the magnetic field dependence of the volume fractions of the AST and MST phases exhibits a distinct magnetic hysteresis with increasing and decreasing magnetic fields. To compare it with the hysteresis observed in the field dependence of the global magnetization, VF_{AST} was plotted along with the normalized $M(H)$ curve obtained in the protocol P1 at $T = 236$ K. The $VF_{AST}(H)$ curve is qualitatively similar to the $M(H)$ curve (see figure 5 for protocol P1; magnetization is normalized with the magnetization at 40 kOe magnetic field). The data for the protocol P2 is not presented here for conciseness. The observation that VF_{AST} and normalized M have similar field dependences confirms that the width of the field induced MST–AST phase transition observed in the global field dependence of the magnetization (and other bulk observables) is due to the nucleation and growth kinetics of this disorder broadened phase transition. It also confirms that the defined threshold voltage used to construct the scanning Hall probe images is realistic.

We further attempt a quantitative analysis of the evolution of the volume fraction of the AST phase as a function of magnetic field. The 'S' shape of the magnetic field dependence of the volume fraction of the AST phase in figure 4 resembles the transformation–time curve predicted by the Avrami model [33], proposed for the crystallization of solids. The central assumption of the Avrami model is that the product phase is nucleated by the germ nuclei which are already present in the parent phase. The density of these germ nuclei decreases in two ways. In the first way some of them become active growth nuclei of the product phase. The second way is the swallowing of other germ nuclei by these growth nuclei in the process of growth. The nucleation events are taken to be totally random. The time dependence of the phase fraction of

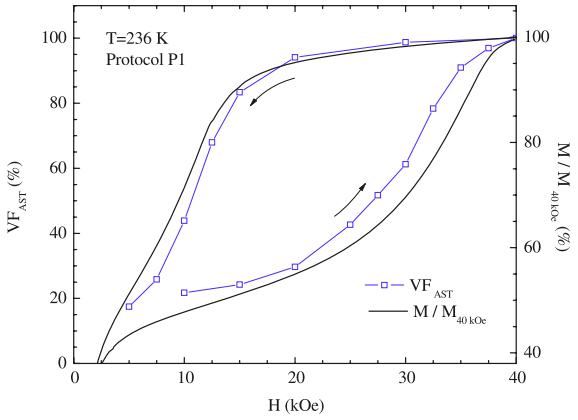

Figure 5. Comparison of the isothermal magnetic field (H) dependence of the volume fraction of the austenite phase (VF_{AST}) and the normalized magnetization ($M/M_{40\ kOe}$) of $Ni_{50}Mn_{34}In_{16}$ alloy at 236 K in protocol P1 (see the text for details).

the product phase is given by the Kolmogorov–Johnson–Mehl–Avrami (KJMA) relation

$$f = 1 - \exp(-kt^n), \tag{1}$$

where k is related to the activation energy and the Avrami exponent n depends on the geometrical factors. Originally the model was proposed for isothermal time dependence of the evolution of the product phase in crystallization from liquid. The model has been extended to the temperature and magnetic field dependence of the phase fraction of the product phase for the first-order phase transition in doped Fe–Rh alloy [34] and the following relationship was found suitable for description of the transition:

$$f = 1 - \exp(-k(T - T_0)^n), \tag{2}$$

where for a temperature driven transition T_0 is the onset temperature of the transition. Similarly, for a magnetic field driven transition the observable T in equation (2) can be replaced by H [34]. We now check whether the KJMA behaviour is observed in the magnetic field dependence of the volume fraction of the AST phase (here the volume fraction is used as the phase fraction). In the original Avrami model and in that used in [34], there is an onset point of transition, i.e. a value of the control variable (time/temperature/magnetic field) up to which the phase fraction of the product phase is zero. However in the present case even at the minimum value of the magnetic field the volume fraction of the product AST phase is non-zero as the sample is already in the phase coexistence region at $T = 236$ K. So we cannot apply the Avrami model directly. We have modified the KJMA relation so as to have a finite value of the volume fraction of the product phase at zero magnetic field. The modified KJMA equation is

$$f = 1 - A\exp(-kH^n), \tag{3}$$

where the factor A is included to allow a finite non-zero value of the phase fraction of the AST phase in zero magnetic field. The fitting of equation (3) with the magnetic field dependence

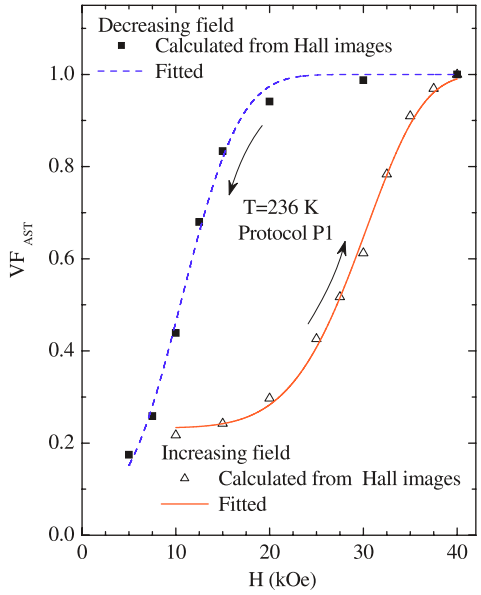

Figure 6. Fitting of the magnetic field (H) dependence of the volume fraction of the austenite phase (VF_{AST}) across the H induced martensite–austenite phase transition at 236 K in protocol P1, using equation (3). See the text for details.

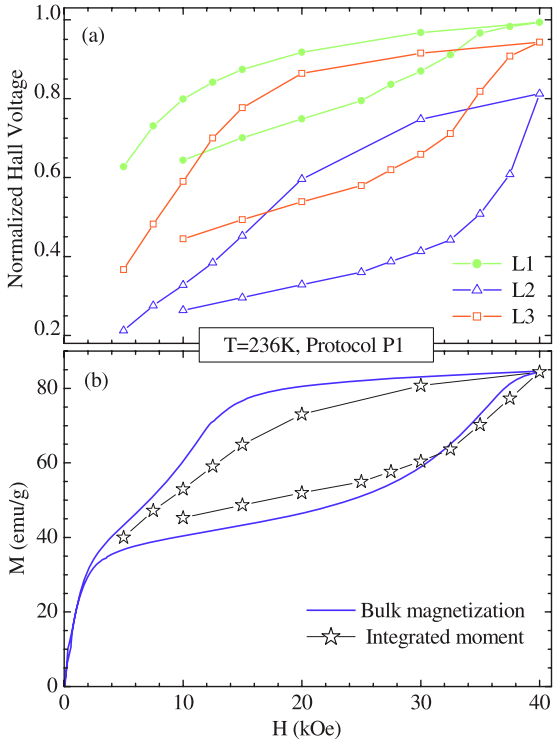

Figure 7. (a) Local Hall voltage versus magnetic field (H) loops at representative sites (L1, L2 and L3) in Hall images at 236 K in protocol P1. The Hall voltage is normalized with its value in a magnetic field of 40 kOe at site L1. (b) Comparison of the H dependence of bulk magnetization (M) measured using the VSM with the integrated moment calculated from Hall images at 236 K in protocol P1. The integrated moment is normalized with the value of M in a magnetic field of 40 kOe. See the text for details.

of VF_{AST} in protocol P1 is presented in figure 6. Clearly, equation (3) fits well with the magnetic field dependence of the volume fraction of the AST phase. The values of A and n (obtained as fitting parameters) in the increasing field cycle are 0.767 and 6.018 respectively. Similarly the values of A and n obtained in the decreasing field cycle are 0.920 and 2.730 respectively. The value of n in the decreasing field cycle is comparable to that obtained for the structural transition in doped Fe–Rh alloy in the increasing/decreasing field cycle [34], but the value of n in the increasing field cycle is larger as compared to that for doped Fe–Rh alloy. Recently such a large value of n (the exponent of the control variable) in a KJMA type of fit is reported for a temperature driven structural transition in uranium [35]. In the present case, the very different values of n in the increasing and decreasing field cycles are due to the different shapes of the $VF_{AST}(H)$ curves in the increasing and decreasing magnetic field cycles. This may be related to the intrinsic asymmetry between supercooling and superheating in the first-order phase transitions [23]. The observation that the volume fraction of the AST phase across the magnetic field induced transition in the present alloy can be fitted with a KJMA type of relation confirms a nucleation and growth mechanism in this magnetic field induced transition.

We now analyse the Hall images further to explore the local magnetic behaviour of the sample across the field driven MST–AST phase transition. This is done by tracking the voltage signal coming from the individual pixels, which corresponds to a 10 μm $\times$ 10 μm sample area, approximately. The field dependence of such a voltage signal produces a local Hall voltage loop. Figure 7(a) presents the local Hall voltage loops corresponding to three representative sites (pixels, named as L1, L2, and L3) on the sample. The Hall voltages in the local loops are normalized to the Hall voltage at the site L1 in 40 kOe magnetic field. It is interesting to observe in figure 7(a) that while the magnetic field induced MST to AST transition is completed well below 40 kOe at the site L1, the transition is probably not completed at the site L2 at $H = 40$ kOe. On the other hand, the transition is very near to completion at the site L3 at the same field value. Further it can be seen that among the three chosen sites, the MST to AST transition is completed first in the increasing magnetic field cycle for the site L1. But the AST to MST transition at this site starts last in the decreasing magnetic field cycle. This sequence is just the reverse for the site L3. The characteristics exhibited by the local Hall voltage loops indicate the presence of a landscape of critical magnetic field for the MST–AST transition across the sample. This kind of disorder induced landscape of transition temperatures or fields had been envisaged earlier theoretically by Imry and Wortis [21], and observed experimentally in vortex matter [22] and various magnetic systems [12, 13]. Thus it confirms the disorder influenced nature of this magnetic field induced MST–AST transition in $Ni_{50}Mn_{34}In_{16}$.

It has been stated in the experimental section above that the magnetic field dependence of the integrated moment is the summation of the signals from all the pixels across the sample. Figure 7(b) shows the comparison of the bulk magnetization measured using the VSM and the integrated

moments calculated from the Hall images. Although the integrated moments calculated from the Hall images follow the bulk magnetization behaviour, there is a visible difference between the two curves. We attribute this difference to the demagnetization factor [36]. While the sample used for the measurements in the VSM has a distorted needle shape, of length approximately 1 mm, the sample used for scanning Hall probe imaging experiments is of the shape of a distorted circular lamina, of diameter approximately 2 mm. The shape of the field dependence of the integrated moments seems to be somewhat different from the individual local loops.

4. Summary and conclusion

We have performed scanning Hall probe imaging experiments on $Ni_{50}Mn_{34}In_{16}$ alloy. The images provide clear visual evidence of the coexistence of the martensite and austenite phases across the magnetic field induced martensite–austenite phase transition in this alloy. This highlights the disorder broadened first-order nature of the phase transition. Thermomagnetic history effects are found to play an important role in the evolution of this phase transition. The phase coexistence regime in $Ni_{50}Mn_{34}In_{16}$ can be reached by changing the applied magnetic field and temperature in different experimental protocols. The relative volume fractions of the martensite and the austenite phases in the phase coexistence regime are found to depend strongly on the path chosen in the field–temperature phase space for varying the temperature and magnetic field. As a result, the functional properties of $Ni_{50}Mn_{34}In_{16}$ also depend on the thermomagnetic history of the sample. Quantitative analysis of the Hall images suggests nucleation and growth dynamics of phases across the magnetic field induced transition. Also the local Hall voltage loops constructed from the Hall images suggest a landscape of the critical field of the MST–AST phase transition, thus confirming the disorder influenced nature of the transition.

References

[1] Sutou Y, Imano Y, Koeda N, Omori T, Kainuma R, Ishida K and Oikawa K 2004 *Appl. Phys. Lett.* **85** 4358

[2] Oikawa K, Ito W, Ymano Y, Sutou Y, Kainuma R, Ishida K, Okamoto S, Kitakami O and Kanomata T 2006 *Appl. Phys. Lett.* **88** 122507

[3] Krenke T, Acet M, Wassermann E F, Moya X, Manosa L and Planes A 2006 *Phys. Rev.* B **73** 174413

[4] Sharma V K, Chattopadhyay M K, Shaeb K H B, Chouhan A and Roy S B 2006 *Appl. Phys. Lett.* **89** 222509

[5] Yu S Y, Liu Z H, Liu G D, Chen J L, Cao Z X, Wu G H, Zhang B and Zhang X 2006 *Appl. Phys. Lett.* **89** 162503

[6] Sharma V K, Chattopadhyay M K and Roy S B 2007 *J. Phys. D: Appl. Phys.* **40** 1869

[7] Krenke T, Duman E, Acet M, Wassermann E F, Moya X, Manosa L, Planes A, Suard E and Ouladdiaf B 2007 *Phys. Rev.* B **75** 104414

[8] Moya X, Mañosa L, Planes A, Aksoy S, Acet M, Wassermann E F and Krenke T 2007 *Phys. Rev.* B **75** 184412

[9] Sharma V K, Chattopadhyay M K, Kumar R, Ganguli T, Tiwari P and Roy S B 2007 *J. Phys.: Condens. Matter* **19** 496207

[10] Sharma V K, Chattopadhyay M K and Roy S B 2007 *Phys. Rev.* B **76** 140401(R)

[11] Roy S B, Chaddah P, Pecharsky V K and Gschneidner K A Jr 2008 *Acta Mater.* **56** 5895

[12] Roy S B, Perkins G K, Chattopadhyay M K, Nigam A K, Sokhey K J S, Chaddah P, Caplin A D and Cohen L F 2004 *Phys. Rev. Lett.* **92** 147203

[13] Moore J D, Perkins G K, Bugoslavsky Y, Cohen L F, Chattopadhyay M K, Roy S B, Chaddah P, Gschneidner K A Jr and Pecharsky V K 2006 *Phys. Rev.* B **73** 144426

[14] Ramos R A, Rikvold P A and Novotny M A 1999 *Phys. Rev.* B **59** 9053

[15] Perkins G K, Moore J, Bugoslavsky Y, Cohen L F, Jun J, Kazakov S M, Karpinski J and Caplin A D 2002 *Supercond. Sci. Technol.* **15** 1156

[16] Chaikin P M and Lubensky T C 1995 *Principles of Condensed Matter Physics* (Cambridge: Cambridge University Press)

[17] Brown P J, Gandy A P, Ishida K, Kainuma R, Kanomata T, Neumann K U, Oikawa K, Ouladdiaf B and Ziebeck K R A 2006 *J. Phys.: Condens. Matter* **18** 2249

[18] Krenke T, Duman E, Acet M, Wassermann E F, Moya X, Manosa L, Planes A, Suard E and Ouladdiaf B 2007 *Phys. Rev.* B **75** 104414

[19] Sharma V K, Chattopadhyay M K and Roy S B 2008 *J. Phys.: Condens. Matter* **20** 425210

[20] White R M and Geballe T H 1979 *Long Range Order in Solids* (New York: Academic)

[21] Imry Y and Wortis M 1979 *Phys. Rev.* B **19** 3580

[22] Soibel A, Zeldov E, Rappaport M, Myasoedov Y, Tamegai T, Ooi S, Konczykowski M and Geshkenbein V B 2000 *Nature* **406** 282

[23] Chattopadhyay M K, Roy S B, Nigam A K, Sokhey K J S and Chaddah P 2003 *Phys. Rev.* B **68** 174404

[24] Roy S B and Chaddah P 2004 *Phase Transit.* **77** 767

[25] Manekar M, Chaudhary S, Chattopadhyay M K, Singh K J, Roy S B and Chaddah P 2002 *J. Phys.: Condens. Matter* **14** 4477

[26] Chattopadhyay M K, Manekar M A, Pecharsky A O, Pecharsky V K, Gschneidner K A Jr, Perkins G K, Bugoslavsky Y V, Roy S B, Chaddah P and Cohen L F 2004 *Phys. Rev.* B **70** 214421

[27] Zhang Y Q, Zhang Z D and Aarts J 2004 *Phys. Rev.* B **70** 132407

[28] Bean C P and Rodbell D S 1962 *Phys. Rev.* **126** 104

[29] Sharma V K and Chattopadhyay M K, unpublished

[30] Chattopadhyay M K, Sharma V K and Roy S B 2008 *Appl. Phys. Lett.* **92** 022503

[31] Sharma V K and Chattopadhyay M K, unpublished

[32] Chattopadhyay M K, Roy S B and Chaddah P 2005 *Phys. Rev.* B **71** 024523

[33] Avrami M 1939 *J. Chem. Phys.* **7** 1103

[34] Manekar M and Roy S B 2008 *J. Phys.: Condens. Matter* **20** 325208

[35] Rai A K, Raju S, Jeyaganesh B, Mohandas E, Sudha R and Ganeshan V 2009 *J. Nucl. Mater.* **383** 215

[36] Joseph R I and Schlomann E 1965 *J. Appl. Phys.* **36** 1579